

On the stability and accuracy of the Empirical Interpolation Method and Gravitational Wave Surrogates

Manuel Tiglio
Aarón Villanueva*

Facultad de Matemática, Astronomía, Física y Computación, Universidad Nacional de Córdoba (5000), Córdoba, Argentina

August, 2020

Abstract

The combination of the Reduced Basis (RB) and the Empirical Interpolation Method (EIM) approaches have produced outstanding results in gravitational wave (GW) science and in many other disciplines. In GW science in particular, these results range from building non-intrusive surrogate models for gravitational waves to fast parameter estimation adding the use of Reduced Order Quadratures. These surrogates have the salient feature of being essentially indistinguishable from or very close to supercomputer simulations of the Einstein equations but can be evaluated in less than a second on a laptop. In this note we analyze in detail how the EIM at each iteration attempts to choose the interpolation nodes so as to make the related Vandermonde-type matrix “as invertible as possible” as well as attempting to optimize the conditioning of its inversion and minimizing a Lebesgue-type constant for accuracy. We then compare through numerical experiments the EIM performance with fully optimized nested variations. We also discuss global optimal solutions through Fekete nodes. We find that in these experiments the EIM is actually close to optimal solutions but can be improved with small variations and relative low computational cost.

1 Introduction

The general problem of determining existence, uniqueness, stability, and accuracy of an optimal interpolant for an arbitrary basis, including the choice of interpolation nodes, is still largely an open one; for recent results in the least squares sense see [1, 2, 3]. The one-dimensional polynomial case is well understood. For example, it is well known that the Chebyshev nodes constitute an optimal solution as they satisfy a min-max property [4]. Yet, Gaussian nodes are not hierarchical (nested), which is in many cases a desired condition.

The multi-dimensional case is more complicated and less developed, as tensor products of one-dimensional polynomials typically suffer from the curse of dimensionality and are also restricted to simple geometries. An active area of research is that one of sparse grids [5]; however, most of the approaches are not nested and in many cases not applicable to complex geometries.

Over the last decade a general quasi-optimal approach for interpolation of parameterized problems, which works extremely well in practice, has gained wide popularity: the Empirical Interpolation Method (EIM) [6, 7, 8]. Given a reduced basis distilled from a parametrized fiducial

*Corresponding author: aaron.villanueva@unc.edu.ar

model, the EIM is, in its original formulation, an efficient algorithm for finding a good set of nodal points and the corresponding interpolant. As of this writing, in GW science the combination of the EIM with a POD or greedy approach to construct reduced bases constitute a powerful way of building accurate surrogate models for binary black holes without any physical approximation [9, 10, 11, 12, 13, 14, 15].

In this note we discuss some fundamental aspects of the EIM as currently used when building gravitational wave surrogates; namely, its stability, accuracy and near-optimality. These features has been observed and discussed at length in the literature of GW surrogates. This note intends to analyze in more detail some technical aspects of the EIM approach as used to date when building GW surrogates. Most of the methodologies here used are actually independent of our application domain of interest and might be useful in other contexts, or even at motivating research at a fundamental level. The approach here adopted is data-driven; that is, no differential equations are invoked.

The structure of this note is as follows. Section 2 briefly reviews the general interpolation problem, while Section 3 discusses the particular case of the EIM approach. Precisely, how it is designed to partially optimize its conditioning (Sec. 3.1) and accuracy (Sec 3.2) and we present variations of it (Sec. 3.3) with “full optimizations” while still following the fundamental steps of the EIM framework. In Section 4 we present results from numerical experiments corresponding to three different cases: i) gravitational waves emitted by black hole collisions, ii) Bessel functions of the first kind, and iii) Legendre polynomials. For each of these cases we numerically compare the conditioning and accuracy of the “standard” EIM with the optimized variations of it. In Section 5 we discuss some issues appearing in the computation of global nodes in the context of GW surrogates and explore partial solutions through Fekete nodes. We close in Section 6 with a summary of our results and some comments.

2 Interpolation.

Since our motivation is that one of gravitational waves we focus on time series – the frequency domain case is identical. Given a set of independent arbitrary basis functions $\{e_i(t)\}_{i=1}^n$ and a function (waveform) $h(t)$, the general interpolation problem consists of finding an interpolant of the form

$$\mathcal{I}_n[h](t) = \sum_{i=1}^n C_i e_i(t), \quad (1)$$

with the interpolation conditions

$$\mathcal{I}_n[h](T_j) = h(T_j), \quad j = 1, \dots, n \quad (2)$$

for a given set of nodes $\{T_j\}$.

The following conditions are in general desired for any interpolation approach:

- Besides existence, preferably the interpolant has to be unique.
- The solution to the problem of defining/finding the location of the interpolation nodes and the interpolant has to be stable/well conditioned.
- The accuracy, when compared to a projection-based approach, has to be competitive.

Some extra conditions to look for might be:

- The interpolation nodes are hierarchical (nested).
- The interpolation problem is fast to solve for.

In this note we discuss some of these points within the context of the EIM.

In the context of the Reduced Basis Method (RBM) framework [16, 17, 18], the functions $e_i(t)$ constitute a set of n basis elements, the *reduced basis*. This basis is found by an earlier implementation of, for example, a greedy or POD algorithm and its span gives a linear approximant to the underlying or fiducial model. Define the $n \times n$ Vandermonde-like matrix (the “V-matrix”) as

$$(\mathbf{V}_n)_{ij} := e_j(T_i).$$

The label n is to keep track of the basis dimension. In this way the interpolation problem can be written as a linear system of the form

$$\sum_{i=1}^n (\mathbf{V}_n)_{ji} C_i = h(T_j), \quad j = 1, \dots, n,$$

which does *not* involve a training set but only knowledge of the reduced basis. This is a highly non-trivial complexity reduction, since if the reduced basis is sparse the interpolation problem is a small one to solve for, unlike the construction of the basis itself, which can be computationally very expensive (see, for example, [19]). In addition, it is also non-trivial that by using only the basis for the construction of the interpolant, the latter has a “good” representation error for *any* function in the space of interest. The intuition is that if the reduced basis is an accurate representation of this space by transitivity so is the interpolant, assuming it was constructed with the choice of good enough interpolating nodes.

If the V-matrix is invertible the solution to the interpolation problem (1,2) is well defined and can be written in a compact manner:

$$\mathcal{I}_n[h](t) = \sum_{i=1}^n B_i(t) h(T_i),$$

with

$$B_i(t) := \sum_{j=1}^n (\mathbf{V}_n^{-1})_{ji} e_j(t).$$

The functions $B_i(t)$ are the generalizations of the Lagrange functions in polynomial interpolation and satisfy $B_i(T_j) = \delta_{ij}$ for $i, j = 1, \dots, n$.

For this note, the items of desired properties of the interpolant therefore reduce to: i) ensure that the V-matrix is not only invertible but also well conditioned, so that the inversion does not amplify numerical errors, ii) analyzing the accuracy and convergence rate of the resulting interpolant.

3 The Empirical Interpolation Method (EIM)

An efficient way of selecting the nodes $\{T_j\}_{j=1}^n$ is by means of the EIM. As described below, the algorithm receives as input the reduced basis and an L -size discretization of the physical domain t . The goal is to find n time nodes $\{T_j\}$ that serve to define the interpolant \mathcal{I}_n through a hierarchical solution of (2).

Algorithm 1 The Empirical Interpolation Method

- 1: **Input:** $\{e_i\}_{i=1}^n, \{t_i\}_{i=1}^L$
 - 2: $T_1 = \operatorname{argmax}_t |e_1|$
 - 3: **for** $j = 2 \rightarrow n$ **do**
 - 4: Build $\mathcal{I}_{j-1}[e_j](t)$
 - 5: $r_j(t) = e_j(t) - \mathcal{I}_{j-1}[e_j](t)$ (where r stands for the *residual*)
 - 6: $T_j = \operatorname{argmax}_t |r_j|$
 - 7: **end for**

 - 8: **Output:** EIM nodes $\{T_i\}_{i=1}^n$ and interpolant \mathcal{I}_n
-

3.1 Conditioning

Besides the requirement of being non-singular, for all practical purposes the V-matrix needs to be well-conditioned to any order n . A matrix is well-conditioned when it does not amplify small errors into large ones when solving a linear problem; in this case the inversion of the matrix itself.

In order to define a suitable quantity to measure this, suppose that \mathbf{V}_n is perturbed as

$$\mathbf{V}_n \rightarrow \mathbf{V}_n + \delta\mathbf{V}_n.$$

This perturbation can be due, for example, to numerical errors, which are always present in practice. Given any induced matrix norm, one can show that

$$\frac{\|(\mathbf{V}_n + \delta\mathbf{V}_n)^{-1} - \mathbf{V}_n^{-1}\|}{\|\mathbf{V}_n^{-1}\|} \leq \kappa(\mathbf{V}_n) \frac{\|\delta\mathbf{V}_n\|}{\|\mathbf{V}_n\|} + \mathcal{O}(\|\delta\mathbf{V}_n\|^2), \quad (3)$$

where we introduce the definition of the condition number of \mathbf{V}_n through

$$\kappa_n := \kappa(\mathbf{V}_n) := \|\mathbf{V}_n\| \|\mathbf{V}_n^{-1}\|. \quad (4)$$

Note that $\kappa(\mathbf{V}_n) \geq 1$.

The definition of a condition number depends not only on the problem but also on the norm used. Throughout this note we always use the 2-norm

$$\|\cdot\| := \|\cdot\|_2,$$

and therefore for brevity we omit from hereon the 2- subscript.

We use the explicit form of the inverse of a matrix in terms of its adjugate

$$\mathbf{V}_n^{-1} = \frac{\operatorname{adj}(\mathbf{V}_n)}{|\det(\mathbf{V}_n)|}$$

to rewrite κ_n as

$$\kappa_n = \frac{\|\mathbf{V}_n\| \|\operatorname{adj}(\mathbf{V}_n)\|}{|\det(\mathbf{V}_n)|}, \quad (5)$$

which later will be useful for our purposes.

The V-matrix is well-conditioned when its condition number $\kappa(\mathbf{V}_n)$ is “small”. Empirically, Vandermonde-like matrices are in general very ill-conditioned [20, 21] except for some particular cases [22]. Although, this does not precludes achieving stability for some matrix inversion algorithms (see for example Björck-Pereyra algorithms [23, 24, 25]). Due to the lack of a general rule

to solve this problem, one can seek for empirical procedures aiming to at least *partially* control the conditioning of these matrices. The EIM is one such approach with impressive results in practice.

The question of how the EIM controls κ of the V-matrix and ensures that it is well defined at each iteration (and exactly what this means) naturally arises. To answer this we begin with an observation about the 5th step of Algorithm 1.

The first iteration implies the construction of the interpolant (Step 4),

$$\mathcal{I}_1[e_2](t) = \frac{e_2(T_1)}{e_1(T_1)}e_1(t),$$

and the associated residual (Step 5),

$$r_2(t) = e_2(t) - \frac{e_2(T_1)}{e_1(T_1)}e_1(t). \quad (6)$$

If we rewrite (6) as

$$r_2(t) = \frac{e_2(t)e_1(T_1) - e_2(T_1)e_1(t)}{e_1(T_1)} \quad (7)$$

we recognize in the numerator the determinant of

$$\mathbf{V}_2(T_1, t) := \begin{pmatrix} e_1(T_1) & e_2(T_1) \\ e_1(t) & e_2(t) \end{pmatrix},$$

that is, \mathbf{V}_2 with T_2 replaced by the free variable t . Denote the determinant of $\mathbf{V}_2(T_1, t)$ by $V_2(T_1, t)$. Then the residual (7) takes the form

$$r_2(t) = \frac{V_2(T_1, t)}{V_1(T_1)}, \quad (8)$$

where $V_1(T_1)$ is the determinant of \mathbf{V}_1 .

Eq. (8) shows that the problem of maximizing $|r_2(t)|$ (Step 6 of the algorithm) is equivalent to that of maximizing $|V_2(T_1, t)|$, since $|V_1(T_1)|$ is a positive constant. Thus, maximize the absolute value of the residual is equivalent to make \mathbf{V}_2 “as invertible as possible”. On the other hand, it also maximizes the denominator of the condition number

$$\kappa(\mathbf{V}_2(T_1, t)) = \frac{\|\mathbf{V}_2(T_1, t)\| \|\text{adj}(\mathbf{V}_2(T_1, t))\|}{|V_2(T_1, t)|}. \quad (9)$$

This does *not* solve the full problem of finding the new node T_2 that minimizes $\kappa(\mathbf{V}_2(T_1, t))$, since the numerator of (9) is not controlled. However, it does a partial job with a low computational cost. Later below we discuss how this partial optimization compares to the full one; that is, the optimization of the full expression of the general version of κ :

$$\kappa(\mathbf{V}_j(T_1, \dots, T_{j-1}, t)) = \frac{\|\mathbf{V}_j(T_1, \dots, T_{j-1}, t)\| \|\text{adj}(\mathbf{V}_j(T_1, \dots, T_{j-1}, t))\|}{|V_j(T_1, \dots, T_{j-1}, t)|}.$$

The observation just made for the first iteration of the EIM is general, as made precise in the following lemma (see the proof in the appendix).

Lemma. Define $\det(\mathbf{V}_j) := V_j(T_1, \dots, T_j)$. Then, the residual $r_j(t)$ computed in the $(j - 1)$ -iteration of the EIM-loop satisfies

$$r_j(t) = \frac{V_j(T_1, \dots, T_{j-1}, t)}{V_{j-1}(T_1, \dots, T_{j-1})} \quad j = 2, 3, \dots, n. \quad (10)$$

As a consequence, once T_j is chosen in Step 6, the residual at this node becomes

$$r_j(T_j) = \frac{V_j(T_1, \dots, T_{j-1}, T_j)}{V_{j-1}(T_1, \dots, T_{j-1})} = \frac{\det(\mathbf{V}_j)}{\det(\mathbf{V}_{j-1})}. \quad (11)$$

This expression tells us that, at each $(j - 1)$ -step, the EIM algorithm selects a new node T_j in order to maximize the module of the determinant of \mathbf{V}_j . This ensures that it will be as invertible as possible while attempting to partially control its conditioning for the next iteration. In this sense the EIM algorithm provides a hierarchical quasi-optimal method to construct stable/well conditioned interpolants.

3.2 Accuracy

So far we have discussed stability/well conditioning. Here we turn into its accuracy, again in the 2-norm. Let's suppose the existence of a parameterized model $h_\lambda(t)$ with λ being a tuple belonging to some compact parameter space. Consider a basis $\{e_i\}_{i=1}^n$, the generated subspace $W_n := \text{Span}\{e_i\}_{i=1}^n$ and a (possibly weighted) scalar product $\langle \cdot, \cdot \rangle$. The optimal linear approximation of the form

$$\sum_{i=1}^n c_i e_i(t)$$

to h_λ is, in the least squares (LS) sense, the orthogonal projection of h_λ onto W_n . If the basis is indeed orthonormal the projection becomes the familiar expression

$$\mathcal{P}_n h_\lambda(t) = \sum_{i=1}^n \langle e_i, h_\lambda \rangle e_i(t). \quad (12)$$

Since (12) is the optimal solution to the LS problem, an interpolant can only have an equal or larger error. To quantify these differences we introduce the Lebesgue constant $^1\Lambda_n$. First, define the discrete norm of a waveform h as

$$\|h\|_d^2 := \sum_{i=1}^L \bar{h}(t_i) h(t_i) \Delta t.$$

Then, the following inequality holds

$$\|h_\lambda - \mathcal{I}_n h_\lambda\|_d \leq \Lambda_n \|h_\lambda - \mathcal{P}_n h_\lambda\|_d \quad \text{where} \quad \Lambda_n := \|\mathcal{I}_n\|_d. \quad (13)$$

When the basis is unitary ($\mathbf{U}\mathbf{U}^\dagger = \mathbf{1}$, with columns storing basis vectors e_i), the following equality is valid in the 2-norm

$$\Lambda_n = \|\mathbf{V}_n^{-1}\| = \max_{\|h\|=1} \left\| \mathbf{V}_n^{-1} h \right\|, \quad (14)$$

If the approximation by projection has fast convergence, the behavior of Λ_n with n may decide how good is the approximation by interpolation. So, it may be desirable to have a slow/controlled growth of Λ_n in order to hopefully mimic the projection approximation and then achieve good convergence rates. In particular, this may be desirable in the case of parameterized problems with some parameter regularity: one expects, in the context of RBM, spectral-type convergence of the

¹The Lebesgue constant is usually defined in the infinity norm. In this note we define it in the 2-norm.

Kolmogorov n -width and, as consequence, of the error decay when using a greedy [26, 27] or POD [28] approach to find the basis.

The Lebesgue constant stated as in (14) is directly related to the condition number $\kappa(\mathbf{V}_n)$ through

$$\kappa(\mathbf{V}_n) = \|\mathbf{V}_n\| \Lambda_n. \quad (15)$$

So, controlling the conditioning of the problem and its accuracy are somewhat related. In the next section we explore variations on the optimization of the EIM aiming to improve this two interrelated aspects of the algorithm: its conditioning and accuracy.

3.3 On optimality

One might wonder how the conditioning and accuracy of the EIM might improve if one replaces the optimization criteria of the EIM algorithm (step 6) by minimizing the condition number of $\mathbf{V}_j(T_1, \dots, T_{j-1}, t)$ or the Lebesgue constant at each step instead of only maximizing its determinant. That is, we consider two variations of the EIM. Instead of choosing

$$T_j = \operatorname{argmax}_t |r_j|,$$

with r_j as in Eq. (10) we consider the following two variations:

1. EIM- κ :

$$T_j = \operatorname{argmin}_t \kappa(\mathbf{V}_j(T_1, \dots, T_{j-1}, t))$$

2. EIM- Λ :

$$T_j = \operatorname{argmin}_t \Lambda_j(t) \quad \text{with} \quad \Lambda_j(t) := \|\mathbf{V}_j^{-1}(T_1, \dots, T_{j-1}, t)\|.$$

That is, at each iteration, EIM- κ and EIM- Λ fully minimize the condition number and Lebesgue constant, respectively. A natural question that arises is how κ and Λ_n behave with the number of basis n , and how they compare with the original EIM. An analytical treatment of this is beyond the scope of this work so we only present numerical results corresponding to distinct cases in Section 4.

As we stated before, this procedure does not solve the full problem since it is still a hierarchical approach: the nodes are nested in each step. One global approach is that one explored in Section 5.

4 Numerical experiments

This section is organized as follows. We present three different experiments applying the optimized algorithms and the EIM in the first three subsections:

1. **Case 1:** The gravitational waves emitted by the collision of two nonspinning black holes in initial quasi-circular orbit for mass ratios $q = m_1/m_2 \in [1, 10]$, in the time range $[-2750, 100]\text{M}$, where M is the total mass of the system and, as is usual in the field, the waveforms were aligned so that $t = 0$ corresponds to the peak of the amplitudes (roughly speaking, the time of coalescence). This corresponds to the model `SpEC_q1_10_NoSpin`[9] from the GWSurrogate Python package [29].
2. **Case 2:** Bessel functions of the first kind, $J_\nu(x)$, in the continuous parameter $\nu \in [0, 50]$ and integration range $x \in [0, 200]$. We compute them using the SciPy library.
3. **Case 3:** Polynomials of degree n , with unity weight in the integration range $x \in [-1, 1]$. That is, a basis composed by Legendre polynomials $L_n(x)$ up to $n = 49$, comparing the results of standard spectral theory using the Gauss-Legendre nodes with those obtained by the EIM and its modified versions.

In all cases we used implementations in Python that we wrote for both the “standard” version of the EIM algorithm and its modifications EIM- κ and EIM- Λ . We also used the package ROMPy [30] to construct the reduced bases used in each example. This package implements a greedy algorithm [10, 9] to construct reduced basis surrogates for one-dimensional parameterized models.

We define the maximum interpolation and projection errors in parameter space at fixed n as $\tilde{\sigma}_n$ and σ_n , respectively. With this notation, Eq. (13) reads

$$\tilde{\sigma}_n \leq \Lambda_n \sigma_n.$$

The summary of our numerical experiments is that, at least in the cases looked at, the optimal variations of the EIM barely show any improvement, both in terms of conditioning and accuracy. In fact, in some steps the original version of the EIM performs better than its optimal variations. This apparent paradox is explained as follows: in both procedures, say, optimizing on Λ_j or κ , a new T_j is found at each $(j - 1)$ -step, but keeping the previous $\{T_i\}_{i=1}^{j-1}$ and, in consequence, \mathbf{V}_{j-1} fixed. Since we are sequentially adding new nodes we are not solving for the global (non-hierarchical problem) but building upon the previous $(j - 1)$ V-matrix. Thus, in principle, there is no reason why fully optimizing at each iteration should give better results, though we would have expected so. Still, this is remarkable, somewhat puzzling, and shows once again the power of the EIM method as largely evidenced in practice. There might be some deeper mathematical reason behind this or it might be a pure coincidence of the cases here looked at, even when they are from very different contexts. A thorough mathematical treatment remains an open question resulting from this note.

4.1 Case 1

The training space was filled with 1001 equispaced complex waveforms

$$h(q, t) := h_+(q, t) + i h_x(q, t)$$

for $(q, t) \in [1, 10] \times [-2750, 100]M$, with time step $\Delta t = 0.1M$. This resulted in 22 basis elements with squared greedy error $\sigma^2 = 1.28 \times 10^{-13}$ ².

Note that the underlying model used to populate the training space is already a surrogate one constructed with the RBM and the EIM. This means that the entire model lives in a finite dimensional function space spanned by a finite basis. This is illustrated in Figure 1. For a greedy tolerance error of 10^{-16} , the number of basis elements n needed to construct a reduced basis for a given training set rapidly reaches the value $n = 23$. The step function behavior of Figure 1 can be explained as follows: if we set the 23 greedy waveforms as our initial training set and next we populate it with arbitrary waveforms from the model, subsequent training spaces will represent linearly dependent waveforms of the 23 initial ones and the curve will become an exact step function.

²We set the tolerance error before reaching double precision so as to avoid roundoff issues.

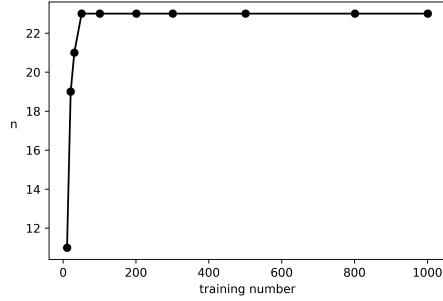


Figure 1: Number of basis elements n vs. the number of training elements associated to equispaced training spaces up to 1001. The step function behavior of the curve is due to the fact that the underlying model to reduce is already spanned by a finite-dimensional space of waveforms.

The three algorithms, EIM, EIM- Λ and EIM- κ choose very similar nodes, in all cases with clustering near the boundaries of the time interval as expected. Figure 2 shows these distributions alongside the curves comparing the behavior of condition number κ with the number of basis elements n for both the EIM and EIM- κ . One can notice that, as expected, the conditioning of the latter does improve, especially at high resolutions.

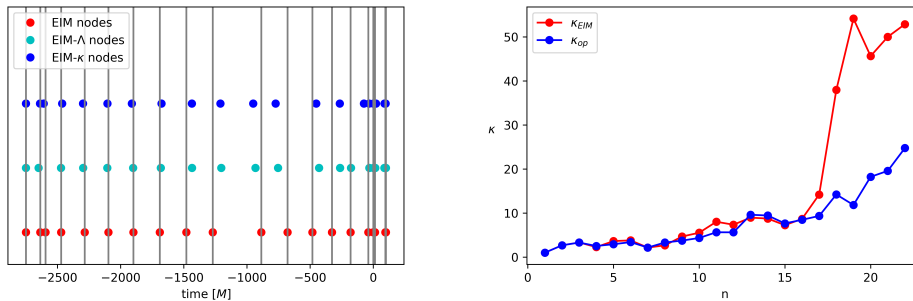


Figure 2: **(Case 1)**. **Left**: Distribution of the 22 interpolation nodes for the three algorithms with vertical lines centered in each EIM node. **Right**: Condition number dependence with basis number n for both EIM and EIM- κ . Note the better behavior of κ for EIM- κ at high resolutions.

Figure 3 shows the dependence of Λ_n with n for both EIM and EIM- Λ . Here there is no improvement; in fact, the EIM performs some times slightly better, sometimes slightly worse than the optimized versions. As was stated above, this is due to the nested character of the algorithms: each step rely on previous nodes to update the next one. The figure also shows the maximum (over the training set) squared interpolation errors $\tilde{\sigma}_n^2$ as a function of n for the three versions of the EIM, and the corresponding RBM squared greedy errors σ_n^2 . The latter, as expected, is a lower bound for all the interpolation approximations; the point to notice is that all curves are very close to each other, suggesting that the EIM is nearly optimal, a rigorous proof of which is not available at this time.

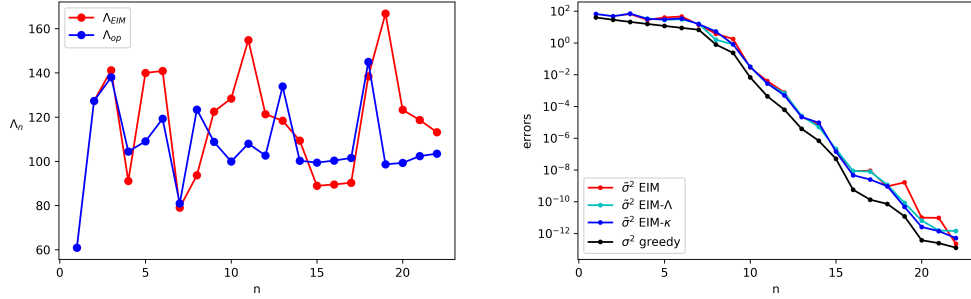


Figure 3: **(Case 1)**. **Left**: Lebesgue constant Λ_n dependence with n for both EIM and EIM- Λ . **Right**: In-sample validation for the three algorithms. Dots correspond to the maximum squared interpolation errors $\tilde{\sigma}_n^2$ and squared greedy errors σ_n^2 . Note that the greedy errors bounds from below the interpolating errors.

The Lebesgue constant provides a bound for the interpolation error in terms of the projection error. Since it is a bound, it is worthwhile looking at the actual errors themselves. Figure 4 shows the quotients between maximum interpolation errors for EIM- Λ and EIM- κ when compared to the original EIM. This figure of merit does show improvements in both variations of the EIM when compared to the latter, even if marginal on average, except for very high accuracy, reaching a peak of 6x improvement.

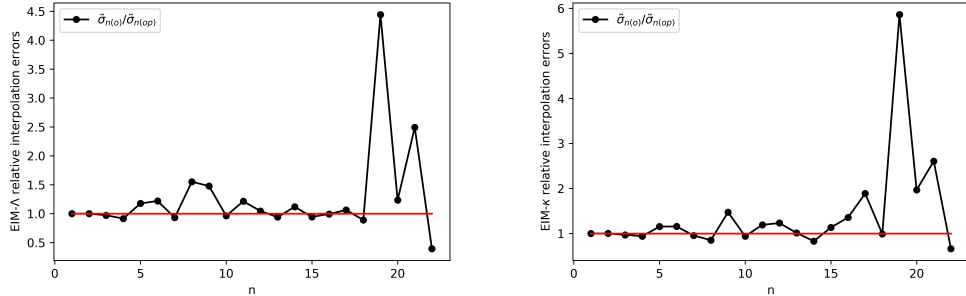


Figure 4: **(Case 1)**. Ratios $\tilde{\sigma}_{n(o)}/\tilde{\sigma}_{n(op)}$ between maximum interpolation errors for original (o) EIM and optimized (op) algorithms. Average values $\langle \tilde{\sigma}_{n(o)}/\tilde{\sigma}_{n(op)} \rangle$ for EIM- Λ and EIM- κ are 1.27 and 1.42, respectively. Besides the fact that the improvements in accuracy are barely better than EIM, the peaks to the end suggest that the optimized algorithms control better the condition number and Lebesgue constant growths close to roundoff.

Since this case, which is within our field of interest, is inconclusive, we next turn to similar studies but using very different function spaces.

4.2 Case 2

The training space is composed of 1001 equispaced Bessel functions in the parameter range $\nu \in [0, 50]$, integration range $x \in [0, 200]$ and discrete spacing $\Delta x = 0.1$. The resulting reduced

basis has 46 elements with squared greedy error $\sigma^2 = 1.55 \times 10^{-15}$.

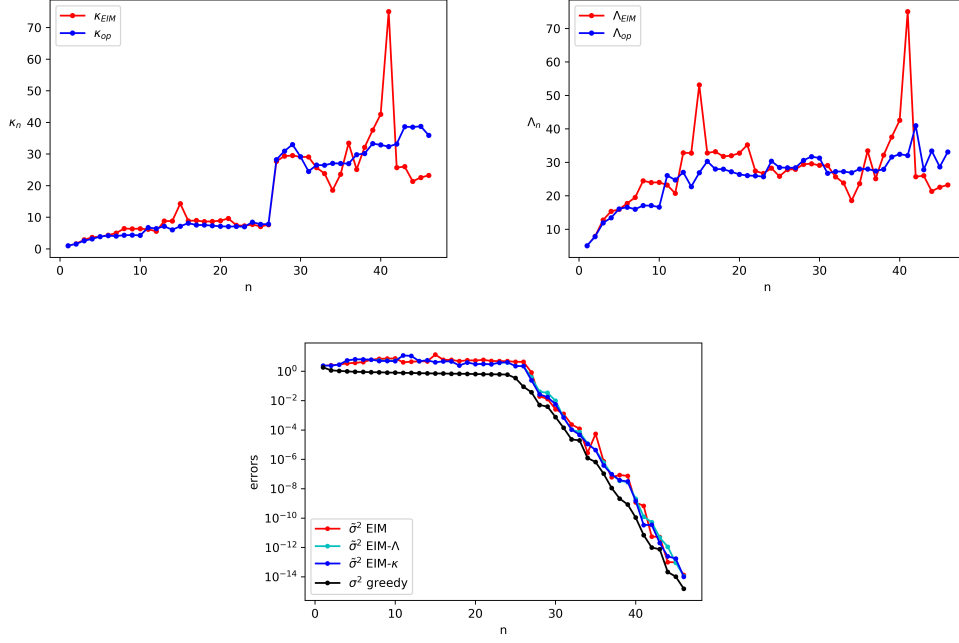


Figure 5: **(Case 2)**. **Upper left**: Condition numbers for both EIM and EIM- κ algorithms. **Upper right**: Lebesgue constants for both EIM and EIM- Λ algorithms. **Bottom**: In-sample validation for the three algorithms and squared greedy errors.

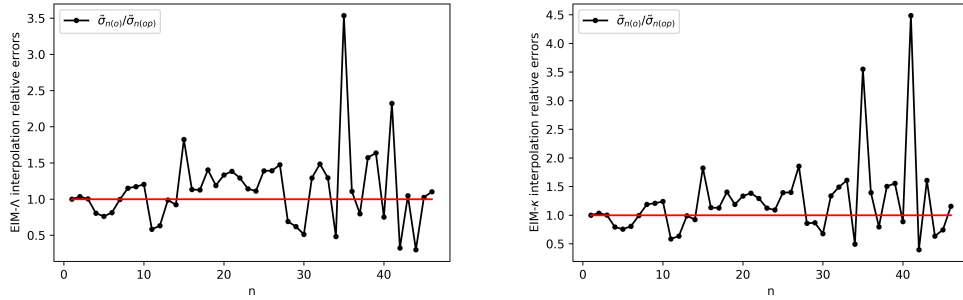


Figure 6: **(Case 2)**. Ratios $\tilde{\sigma}_{n(o)}/\tilde{\sigma}_{n(op)}$ between maximum interpolation errors for original (o) EIM and optimized (op) algorithms. Mean values $\langle \tilde{\sigma}_{n(o)}/\tilde{\sigma}_{n(op)} \rangle$ for EIM- Λ and EIM- κ are 1.13 and 1.23, respectively.

4.3 Case 3

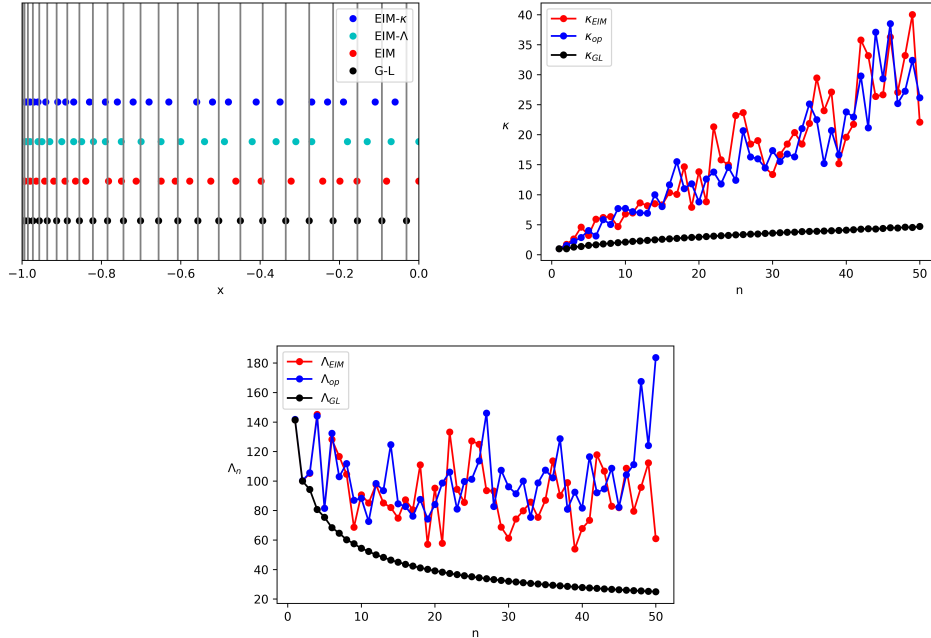


Figure 7: (**Case 3**). **Upper Left**: Distribution of nodes in the interval $[-1, 0]$ for the three algorithms compared with the Gauss-Legendre (G-L) quadrature nodes from classical polynomial interpolation. **Upper Right** and **Bottom**: Condition numbers and Lebesgue constants in function of n for EIM, EIM- κ and EIM- Λ against to those corresponding to G-L nodes.

In Figure 7 we show the distribution of nodes in the semi-interval $[-1, 0]$ (Gauss-Legendre nodes are symmetrical with respect to the origin). We point out that the EIM, EIM- κ and EIM- Λ nodes are almost (instead of exactly) symmetrical with respect to the origin. In the figure showing Lebesgue constants for the three cases, although one may expect an increasing (logarithmic) behavior of Λ_n , we remark that these Lebesgue constants are computed in the 2-norm, and in fact this slow decay is consistent with other results in the literature; see for example Figure 8 of [31].

In this experiment the optimized algorithms do not show any improvement in κ and Λ against EIM for Legendre polynomial basis. The better behavior of both the condition number and Lebesgue constants for Gauss-Legendre nodes is noticeable.

5 On global nodes

Nesting may be a desired property of algorithms when one looks for a trade-off between cost and accuracy and global procedures are already expensive to implement. In the case of general interpolation, this requirement (nesting) might become in some cases mandatory in practice. For example, consider the following problems:

1. Given a fiducial model, the search for a reduced order model belonging to the best approximation linear space (Kolmogorov-type problem, see [32, 33, 34]).

2. The computation of global minima for Lebesgue constants, which controls the stability ([18], p. 278) and accuracy of the interpolation³.
3. The computation of global minima for the condition number κ corresponding to V-matrices.
4. The computation of global maxima for the Fekete function defined as

$$F_n(t_1, \dots, t_n) := |\det(\mathbf{V}_n(t_1, \dots, t_n))|.$$

In polynomial interpolation these global maxima are known as the *Fekete points* [37], here we will follow the same notation for any set of bases.

Problem 1) is computationally hard in the sense that it carries a combinatorial cost $\mathcal{O}(n!)$ but greedy-type implementations (e.g. RBM, see Ref. [38] and citations therein) are well suited for this, minimizing the computational burden down to (or close to) a linear one. Problems 2) and 3) were partially faced in this note with the adoption of a nesting approach to find good interpolating nodes. Problem 4), on the other hand, is half way in the sense that it still poses the challenge of a global optimization but over a less complex function than in 2) and 3), namely: the Fekete function.

Fekete points. As we saw in Section 3.1, the Fekete function appears in the denominator of the condition number (and Lebesgue constant) evaluated at EIM nodes. These nodes are quasi-optimal in the sense that they constitute nested optimizations of the Fekete function. Otherwise, global optimization is achieved through Fekete points. The relevance of Fekete points originally came from polynomial interpolation. They impose an upper bound to the Lebesgue constant in the infinity norm, $\Lambda_{n,\infty} \leq n$ [37]. But, actually, this bound is general in the sense that its proof does not rely on the form of the basis functions themselves. These points are known analytically only in few domains, for example in the real interval they correspond to the Gauss-Legendre-Lobatto points[37]). In data-driven methods, counting with discrete training spaces for building models, these questions can be explored only numerically.

Gravitational waves. In the context of Reduced Basis, one may ask for Fekete points for GW surrogates. This problem can evolve into a hard one with the increase of reduced space dimensionality. Just note that the coalescence of two black holes is defined by an 8-dimensional parameter space and actual reduced order models for the emitted gravitational waves deal with reduced dimensionality of order $\sim 10^2$ [12]. In this section we explore these issues for Case 1, which is a considerably smaller problem yet computationally challenging.

³These points are commonly known in polynomial interpolation as the *Lebesgue points*, and they are not known theoretically even for the real interval [35, 36]

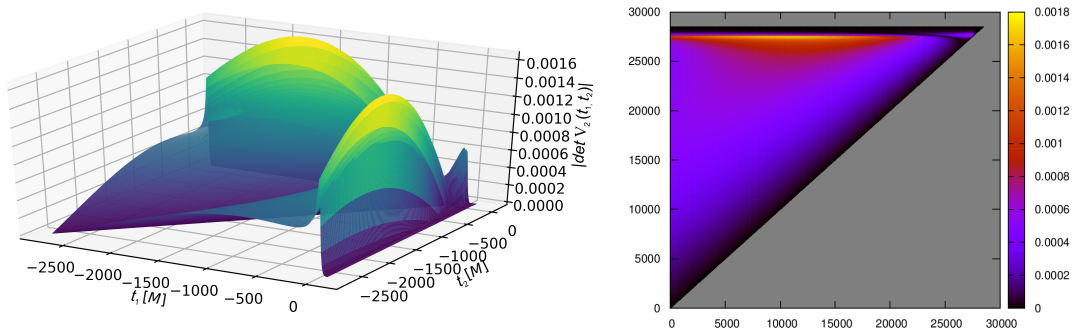


Figure 8: **(Left)**. Surface representation of the two dimensional Fekete function $F_2(t_1, t_2)$ corresponding to Case 1 of Section 4. **(Right)**. Projection of the surface on the plane. Axes represent the common interval $[-2750, 100]M$ with points enumerated from 0 to 28500. We show only the upper triangular domain since $F_2(t_1, t_2)$ is symmetric in its two variables.

As a mode of illustration, we plot in Figure 8 (left) the surface corresponding to Fekete function

$$F_2(t_1, t_2) = |\det(\mathbf{V}_2(t_1, t_2))|$$

for two reduced bases for the gravitational waves of Case 1. Since the general Fekete function $F_n(t_1, \dots, t_n)$ is symmetrical with respect to the exchange of variables, only one of the two triangular regions is shown in the color map of Figure 8. The map shows two regions where Fekete function is non-zero separated by a zero (or close to zero) dark interface on the right corner. Then we have two local maxima and one may compute them directly by brute force.

We computed Fekete points for the GW reduced basis using the following methodology: first, we get local maxima for Fekete function F_n using the modified Powell algorithm [39] implemented in the Scipy optimization module [40]. We use the first n EIM nodes as seeds in each case to start the algorithm. We computed a total of 14 local maxima with this method. Finally, we validated Fekete nodes using the SHGO algorithm [41] for global optimization implemented in [40] to compute all local maxima. In this context, validation means to compute all local maxima and ensure that they fall below the corresponding EIM-seeded ones. We use the Sobol sampling method and allow the symmetry option to reduce the search space by $\mathcal{O}(n!)$ (note that the symmetry regions for arbitrary n correspond to $n!$ simplexes). We used a CPU intel CORE i5 with 4GB RAM, being able to validate Fekete points up to $n = 7$ due to the increasing computation wall time. This can be seen in Figure 9.

All local maxima computed with the SHGO algorithm fall below the corresponding EIM-seeded local maxima. This suggests that the EIM algorithm seems to localize the most important regions in simplexes in which to look up for Fekete points. Also notice the semi-logarithmic behavior of the function values F_n evaluated at Fekete nodes, suggesting a direct extrapolation from the 7 validated global maxima to the remaining non-validated Fekete nodes.

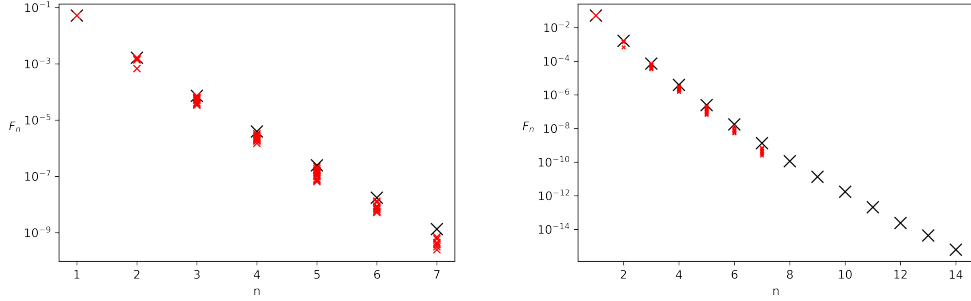


Figure 9: Fekete function values (**black** crosses) at local maxima seeded with EIM nodes for $n = 1, 2, \dots, 14$. They were computed with an implementation of the modified Powell algorithm from the Scipy optimization module. We validated Fekete points with the SHGO algorithm to compute local maxima (**red** crosses) up to $n = 7$. Note all local maxima (red) fall below EIM-seeded local maxima (black).

The EIM nodes seem to be good seeds for optimization in this example and the computed Fekete nodes do not differ too much from them. For example, in the $n = 2$ case, the EIM nodes correspond to $T_0 = -0.2M$ and $T_1 = -1690.8M$. Seeding the algorithm with these points we get the optimized ones $T_0^{opt} = -0.7M$ and $T_1^{opt} = -1690.8M$ in which the Fekete function reaches the value 1.6×10^{-3} . This feature remains up to $n = 14$: local maxima do not end up far from EIM-seeds. To see this, we computed euclidian distances d between EIM seeds and the corresponding local maxima. Also we computed relative distances with respect to the whole time interval $[-2750, 100]M$. See Table below.

n	d/M	rel. d	n	d/M	rel. d
2	3.415	0.120%	9	175	6.13%
3	535	0.189%	10	226	7.92%
4	135	4.72%	11	370	13.0%
5	281	9.86%	12	280	9.83%
6	510	17.9%	13	217	7.60%
7	207	7.25%	14	316	11.1%
8	368	12.9%			

6 Final comments

We explored two different optimization criteria applied to nested variations of the EIM. This was suggested by a link between the EIM and the determinant of the Vandermonde matrix. We optimized on the condition number of the Vandermonde matrix and the Lebesgue constant, both in the 2-norm. For the EIM applied to GWs, we have found a sudden growth of the condition number κ at high resolutions (see Figure 2), which can be avoided through a simple modification of the algorithm in selecting the interpolation nodes. This result suggests that it might be worthwhile keeping in mind this growth when working with high accuracy.

The slow growth of the Lebesgue-type constant in the EIM is consistent with other results, for example see Figure 8 of [31]. In our numerical experiments (see Cases 1 and 2) the condition number for the optimized code is better controlled at high resolution than in the EIM and the interpolation seems to work better in average at these stages.

Motivated by the link mentioned above, we also computed Fekete points for GWs and found that EIM nodes are good seeds to instantiate local optimization algorithms. At least in this case, EIM nodes seem to localize the best regions in physical space to look up for global nodes for the Fekete function.

As a summary, this note presents further evidence that a nearly optimal convergence rate rigorous proof, similar to that one of the greedy RBM [16, 17, 18], might be shown.

Acknowledgments

We thank Jorge Pullin, the Horace Hearne Institute and the Center for Computation and Technology at LSU, for hospitality while part of this work was done. We also thank Scott Field and Stephen Lau for valuable comments on a previous version of this manuscript. This work was supported partially by CONICET and EVC-CIN (Argentina).

A Proof of the Lemma

Consider the nested matrix $\mathbf{V}_j(t)$ defined as

$$\mathbf{V}_j(t) := \begin{pmatrix} & & & e_j(T_1) \\ & \mathbf{V}_{j-1} & & e_j(T_2) \\ & & & \vdots \\ e_1(t) & e_2(t) & \cdots & e_j(t) \end{pmatrix},$$

where \mathbf{V}_{j-1} is the $(j-1)$ -order V-matrix associated to the empirical nodes T_1, \dots, T_{j-1} . That is, $\mathbf{V}_j(t)$ is \mathbf{V}_j with T_j replaced by t . Write the determinant of $\mathbf{V}_j(t)$ as

$$V_j(T_1, \dots, T_{j-1}, t) = e_j(t) \det(\mathbf{V}_{j-1}) + e_j(T_{j-1}) C_{j-1n}[\mathbf{V}_j(t)] + \dots + e_j(T_1) C_{1j}[\mathbf{V}_j(t)], \quad (16)$$

where

$$C_{ik}[\cdot] = (-1)^{i+k} D_{ik}[\cdot]$$

denotes the (i, k) -cofactor of $[\cdot]$, and $D_{ik}[\cdot]$ denotes the determinant of $[\cdot]$ after eliminating its i -th row and j -th column.

Divide (16) by $\det(\mathbf{V}_{j-1}) = V_{j-1}(T_1, \dots, T_{j-1})^4$

$$\frac{V_j(T_1, \dots, T_{j-1}, t)}{V_{j-1}(T_1, \dots, T_{j-1})} = e_j(t) - \frac{1}{\det(\mathbf{V}_{j-1})} \left\{ e_j(T_{j-1}) D_{j-1j}[\mathbf{V}_j(t)] + \dots \right. \\ \left. + (-1)^j e_j(T_1) D_{1j}[\mathbf{V}_j(t)] \right\}. \quad (17)$$

Let's write the subtracting term of the r.h.s. of (17) in matrix notation,

$$\frac{1}{\det(\mathbf{V}_{j-1})} \left((-1)^j D_{1j}[\mathbf{V}_j(t)] \quad \cdots \quad D_{j-1j}[\mathbf{V}_j(t)] \right) \begin{pmatrix} e_j(T_1) \\ \vdots \\ e_j(T_{j-1}) \end{pmatrix}. \quad (18)$$

⁴The EIM-loop ensures, by independence of row and column vectors, that the determinant of the V-matrix is non zero to any order $j \geq 1$.

Now write the interpolant $\mathcal{I}_{j-1}[e_j](t)$ in the same spirit,

$$\begin{aligned}\mathcal{I}_{j-1}[e_j](t) &= (e_1(t) \quad \dots \quad e_{j-1}(t)) \mathbf{V}_{j-1}^{-1} \begin{pmatrix} e_j(T_1) \\ \vdots \\ e_j(T_{j-1}) \end{pmatrix} \\ &= \frac{1}{\det(\mathbf{V}_{j-1})} (e_1(t) \quad \dots \quad e_{j-1}(t)) \operatorname{adj}(\mathbf{V}_{j-1}) \begin{pmatrix} e_j(T_1) \\ \vdots \\ e_j(T_{j-1}) \end{pmatrix}.\end{aligned}$$

This is similar to expression 18 above. If one proves that

$$\left((-1)^j D_{1j}[\mathbf{V}_j(t)] \quad \dots \quad D_{j-1j}[\mathbf{V}_j(t)] \right) \quad (19)$$

is equal to

$$(P_1(t) \quad \dots \quad P_{j-1}(t)) := (e_1(t) \quad \dots \quad e_{j-1}(t)) \operatorname{adj}(\mathbf{V}_{j-1}), \quad (20)$$

the proof of formula 10 will be completed. Let's look at the first component of (19):

$$(-1)^j D_{1j}[\mathbf{V}_j(t)] = \sum_{i=1}^{j-1} (-1)^{i-1} e_i(t) D_{j-1i}[\mathbf{V}_j(t)(1|j)],$$

where $\mathbf{V}_j(t)(1|j)$ stands for $\mathbf{V}_j(t)$ without its 1-th row and j -th column. On the other hand, the first element of (20) is equal to

$$\begin{aligned}P_1(t) &= \sum_{i=1}^{j-1} e_i(t) (\operatorname{adj}(\mathbf{V}_{j-1}))_{i1} = \sum_{i=1}^{j-1} e_i(t) C_{1i}(\mathbf{V}_{j-1}) \\ &= \sum_{i=1}^{j-1} (-1)^{i-1} e_i(t) D_{1i}(\mathbf{V}_{j-1}).\end{aligned}$$

Finally, notice that

$$D_{j-1i}[\mathbf{V}_j(t)(1|j)] = D_{1i}(\mathbf{V}_{j-1}).$$

Therefore

$$(-1)^j D_{1j}(\mathbf{V}_j(t)) = P_1(t)$$

and, in the same way,

$$(-1)^{j-1-i} D_{ij}(\mathbf{V}_j(t)) = P_i(t) \quad \text{for } i = 1, \dots, j-1.$$

Therefore $\mathcal{I}_{j-1}[e_j](t)$ is equal to expression 18:

$$\frac{V_j(T_1, \dots, T_{j-1}, t)}{V_{j-1}(T_1, \dots, T_{j-1})} = e_j(t) - \mathcal{I}_{j-1}[e_j](t) = r_j(t)$$

and the Lemma is proved.

References

- [1] Cohen, A., Davenport, M. A. & Leviatan, D. On the stability and accuracy of least squares approximations. *Foundations of Computational Mathematics* **13**, 819–834 (2013).
- [2] Cohen, A., Davenport, M. A. & Leviatan, D. Correction to: on the stability and accuracy of least squares approximations. *Foundations of Computational Mathematics* **19**, 239 (2019).
- [3] Cohen, A. & Migliorati, G. Optimal weighted least-squares methods. *The SMAI journal of computational mathematics* **3**, 181–203 (2017).
- [4] Deuffhard, P. & Hohmann, A. *Numerical Analysis in Modern Scientific Computing: An Introduction*, vol. 43 (Springer, 2003).
- [5] Garcke, J. & Griebel, M. Sparse grids and applications. *Lecture Notes in Computational Science and Engineering* **88** (2013).
- [6] Maday, Y., Nguyen, N. C., Patera, A. T. & Pau, S. H. A general multipurpose interpolation procedure: the magic points. *Communications on Pure and Applied Analysis* **8**, 383–404 (2009).
- [7] Barrault, M., Maday, Y., Nguyen, N. C. & Patera, A. T. An empirical interpolation method: application to efficient reduced-basis discretization of partial differential equations. *Comptes Rendus Mathématique* **339**, 667 – 672 (2004).
- [8] Chaturantabut, S. & Sorensen, D. Nonlinear model reduction via discrete empirical interpolation. *SIAM J. Scientific Computing* **32**, 2737–2764 (2010).
- [9] Blackman, J. *et al.* Fast and accurate prediction of numerical relativity waveforms from binary black hole coalescences using surrogate models. *Phys. Rev. Lett.* **115**, 121102 (2015).
- [10] Field, S. E., Galley, C. R., Hesthaven, J. S., Kaye, J. & Tiglio, M. Fast prediction and evaluation of gravitational waveforms using surrogate models. *Phys. Rev. X* **4**, 031006 (2014).
- [11] Blackman, J. *et al.* Numerical relativity waveform surrogate model for generically precessing binary black hole mergers. *Phys. Rev. D* **96**, 024058 (2017).
- [12] Blackman, J. *et al.* A surrogate model of gravitational waveforms from numerical relativity simulations of precessing binary black hole mergers. *Phys. Rev. D* **95**, 104023 (2017).
- [13] Varma, V. *et al.* Surrogate models for precessing binary black hole simulations with unequal masses. *Phys. Rev. Research*. **1**, 033015 (2019).
- [14] Varma, V. *et al.* Surrogate model of hybridized numerical relativity binary black hole waveforms. *Phys. Rev. D* **99**, 064045 (2019).
- [15] Varma, V. *et al.* Surrogate models for precessing binary black hole simulations with unequal masses. *Phys. Rev. Research* **1**, 033015 (2019).
- [16] Prud'homme, C. *et al.* Reliable real-time solution of parametrized partial differential equations: Reduced-basis output bound methods. *Journal of Fluids Engineering* **124**, 70 (2002).
- [17] Hesthaven, J., Rozza, G. & Stamm, B. *Certified Reduced Basis Methods for Parametrized Partial Differential Equations*. SpringerBriefs in Mathematics (Springer International Publishing, 2015).

- [18] Quarteroni, A., Manzoni, A. & Negri, F. *Reduced Basis Methods for Partial Differential Equations: An Introduction*. UNITEXT (Springer International Publishing, 2015).
- [19] Cohen, A., Dahmen, W., DeVore, R. & Nichols, J. Reduced basis greedy selection using random training sets. *ESAIM: M2AN* **54**, 1509–1524 (2020).
- [20] Gautschi, W. How (un)stable are Vandermonde systems? In *International Symposium on Asymptotic and Computational Analysis: Conference in Honor Frank W. J. Olvers 65th Birthday* (R. Wong, editor), vol. 124 of *Lecture Notes in Pure and Applied Mathematics*, 193210 (Marcel Dekker, New York, 1990).
- [21] Boyd, J. P. & Gildersleeve, K. W. Numerical experiments on the condition number of the interpolation matrices for radial basis functions. *Applied Numerical Mathematics* **61**, 443 – 459 (2011).
- [22] Pan, V. Y. How bad are Vandermonde matrices? *SIAM J. Matrix Analysis Applications* **37**, 676–694 (2015).
- [23] Björck, A. & Pereyra, V. Solutions of Vandermonde systems of equations. *Mathematical Programming* **24**, 893–903 (1970).
- [24] Higham, N. Error analysis of the Björck-Pereyra algorithms for solving Vandermonde systems. *Numerische Mathematik* **50**, 613–632 (1987).
- [25] Dahlquist, G. & Björck, A. *Numerical Methods in Scientific Computing, Volume I* (Society for Industrial and Applied Mathematics, 2008).
- [26] Binev, P. *et al.* Convergence rates for greedy algorithms in reduced basis methods. *SIAM J. Math. Analysis* **43**, 1457–1472 (2011).
- [27] DeVore, R., Petrova, G. & Wojtaszczyk, P. Greedy algorithms for reduced bases in banach spaces. *Constructive Approximation* **37** (2012).
- [28] Haasdonk, B. Convergence rates of the podgreedy method. *European Series in Applied and Industrial Mathematics (ESAIM): Mathematical Modelling and Numerical Analysis* **47** (2013).
- [29] gwsurrogate 1.0.6. URL <https://pypi.org/project/gwsurrogate/>.
- [30] ROMPy package. URL <https://bitbucket.org/chadgalley/rompy/src/master/>.
- [31] Maday, Y. & Mula, O. *A Generalized Empirical Interpolation Method: Application of Reduced Basis Techniques to Data Assimilation*, 221–235 (Springer Milan, Milano, 2013).
- [32] Magaril-Il’yaev, G. G., Osipenko, K. Y. & Tikhomirov, V. M. On exact values of n-widths in a Hilbert space. *Journal of Approximation Theory* **108**, 97 – 117 (2001).
- [33] Nguyen, V. K. Greedy algorithms and Kolmogorov widths in Banach spaces. *Journal of Approximation Theory* **251**, 105344 (2020).
- [34] Wojtaszczyk, P. On greedy algorithm approximating kolmogorov widths in banach spaces. *Journal of Mathematical Analysis and Applications* **424**, 685 – 695 (2015).
- [35] Briani, M., Sommariva, A. & Vianello, M. Computing Fekete and Lebesgue points: Simplex, square, disk. *Journal of Computational and Applied Mathematics* **236**, 2477 – 2486 (2012).
- [36] Boyd, J. A numerical comparison of seven grids for polynomial interpolation on the interval. *Computers and Mathematics with Applications* **38**, 35 – 50 (1999).

- [37] Canuto, C., Hussaini, M., Quarteroni, A. & Zang, T. *Spectral Methods: Fundamentals in Single Domains*, vol. 23 (2006).
- [38] Hesthaven, J. S., Rozza, G. & Stamm, B. *Certified Reduced Basis Methods for Parametrized Partial Differential Equations*. Springer Briefs in Mathematics (Springer, Switzerland, 2015), 1 edn.
- [39] Powell, M. J. D. An efficient method for finding the minimum of a function of several variables without calculating derivatives. *The Computer Journal* **7**, 155–162 (1964).
- [40] Optimization (scipy.optimize). URL <https://docs.scipy.org/doc/scipy/reference/tutorial/optimize.html>.
- [41] Endres, S., Sandrock, C. & Focke, W. A simplicial homology algorithm for Lipschitz optimisation. *Journal of Global Optimization* (2018).